

Driven reconnection in a quadrupole cusp field

A. Y. Aydemir

Institute for Fusion Studies, The University of Texas at Austin, Austin, Texas 78712

(Received 13 June 2005; accepted 20 July 2005; published online 19 August 2005)

Driven magnetic reconnection in a quadrupole cusp field is examined numerically in various collisionality regimes. Quasi-steady-state reconnection rates far in excess of often-quoted limits are observed. As expected, the rate is determined by external boundary conditions and appears to be limited only by computational concerns; thus, in this configuration the slow reconnection is differentiated from the fast one only by changes in the reconnection-layer geometry. Collisional reconnection exhibits the typical extended current layer of the Sweet-Parker model, whereas the collisionless reconnection mediated by kinetic-Alfvén or whistler waves has the Petschek-type “X-layer” configuration. The current density at the X point is reduced in the collisionless cases, in qualitative agreement with the results from the Versatile Toroidal Facility experiment. © 2005 American Institute of Physics. [DOI: 10.1063/1.2032647]

Magnetic reconnection changes topology of magnetic fields embedded in highly conducting plasmas and is instrumental in converting some of the stored energy in the field into the kinetic and internal energies of the plasma. It has been studied extensively in laboratory, geophysical, and astrophysical contexts and is now the subject of entire monographs.^{1,2} Although early discussions were carried out mainly in terms of resistive (collisional) magnetohydrodynamic (MHD) models, more recent works have focused on the role of collisionless and related physics brought in by extensions of resistive MHD. Some of the recent advances are discussed by Biskamp *et al.*³ and Bhattacharjee *et al.*⁴

From the very beginning, the rate of reconnection and the associated reconnection-layer geometry have been the focus of inquiry, and various answers, based mostly on phenomenological arguments, have been proposed. Of these, the best known are the Sweet-Parker current sheet model,^{5,6} which predicts a rate that scales as $\eta^{1/2}$, where η is a measure of the resistivity in the reconnection layer, and the Petschek model,⁷ which predicts a much weaker, logarithmic, dependence on resistivity. The former is usually considered to be too slow, especially to explain the energetics of solar flares, its original goal, and the latter is considered unphysical, since it ignores the essential physics of the diffusion layer.

A physical system in which magnetic-field lines go through a topology change can be conceptually divided into two sections: an inner “reconnection region” that includes the reconnection layer (where the ideal MHD assumption breaks down) and its immediate surroundings, and an outer region that provides the drive for reconnection, a source of mechanical or potential energy. In this sense, reconnection is always a driven process, and the rate of reconnection is a function, not only of the physics of the inner region, but also of the strength of the drive that originates outside. Thus, limits on reconnection rates can only be studied accurately in cases where this conceptual division is also introduced physically, separating and isolating the driver from the driven inner section.

An example of an unambiguously driven physical system is the Versatile Toroidal Facility (VTF) experiment,⁸ where the reconnection drive is an externally generated inductive electric field in a separately produced quadrupolar cusp field (the new closed cusp geometry of VTF is not addressed in this work). Our goal here is to study magnetic reconnection numerically in a similar system, but in two dimensions. The quadrupole field geometry used in our studies is shown in Fig. 1.

For our work we use a number of different but related models to describe the reconnection dynamics in various collisionality regimes. The first is a reduced two-fluid model that retains the electron inertia and electron pressure terms in a generalized Ohm’s law. It has been discussed extensively in the literature⁹ and is presented here without discussion:

$$\frac{dU}{dt} = [J, \psi] + \mu \nabla_{\perp}^2 U, \quad (1)$$

$$\frac{dF}{dt} = \rho_s^2 [U, \psi] + \eta \nabla_{\perp}^2 \psi - \nu \nabla_{\perp}^4 \psi. \quad (2)$$

The magnetic field is of the form $\mathbf{B} = B_z \mathbf{e}_z + \nabla \psi \times \mathbf{e}_z$, where B_z is a strong “guide field” in the symmetry direction \mathbf{e}_z . The fluid velocity is given by $\mathbf{v} = \mathbf{e}_z \times \nabla \phi$, and the Poisson brackets are defined by $[A, B] = \mathbf{e}_z \cdot \nabla A \times \nabla B$. For any scalar A , we define $dA/dt \equiv \partial A / \partial t + [\phi, A]$. The fluid vorticity is given by $U = \nabla^2 \phi$, and the current density is $\mathbf{J} = -\nabla^2 \psi$. The generalized flux function $F \equiv \psi + d_e^2 J$ represents the axial component of the canonical momentum. The electron skin depth is $d_e = c / \omega_{pe}$, and $\rho_s = \sqrt{T_e / m_i} / \omega_{ci}$ is the ion sound length, or the ion gyroradius at the electron temperature. The lengths are typically normalized to the system size $L \equiv L_x = L_y$, and times are given in units of the Alfvén time $\tau_A = L / v_A$, where $v_A = B_z / \sqrt{\mu_0 \rho}$. Quantities with the subscript “ ∞ ” refer to values at the computational boundary. The viscosity (μ) term is included for numerical reasons. The anomalous electron viscosity (or hyper-resistivity) term (ν) will be shown to play a crucial role in balancing the applied electric field in collisionless calculations, although it is included in all cases.

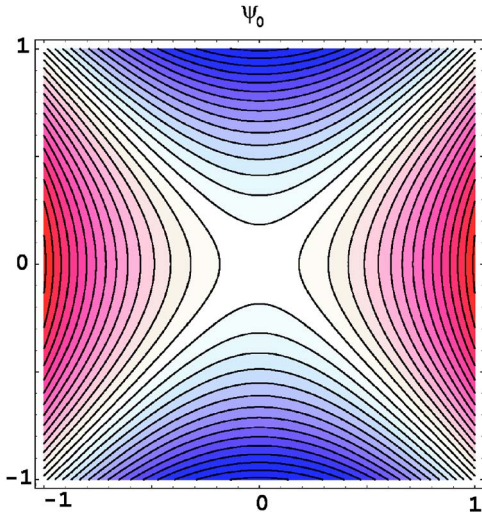


FIG. 1. (Color online) Initial quadrupolar field geometry with a center X point used in the numerical studies.

Note that by letting $d_e = \rho_s = 0$ in Eq. (2), we obtain the usual two-dimensional (2D) reduced, resistive MHD model, used in our purely resistive calculations.

The second model is a Hall MHD (HMHD) system that ignores electron inertia and pressure terms ($d_e = \rho_s = 0$) in the generalized Ohm's law but adds the ion skin-depth length scale $d_i = c/\omega_{pi}$. The particular form of the equations given below is due to Fitzpatrick,¹⁰ with a slightly different sign convention:

$$\frac{dU}{dt} = [J, \psi] + \mu \nabla_{\perp}^2 U, \quad (3)$$

$$\frac{d\psi}{dt} = d_i [\psi, B_z] + \eta \nabla_{\perp}^2 \psi - \nu \nabla_{\perp}^4 \psi, \quad (4)$$

$$\frac{dV_z}{dt} = [B_z, \psi] + \mu \nabla_{\perp}^2 V_z, \quad (5)$$

$$\frac{dB_z}{dt} = [V_z, \psi] + d_i [\psi, J] + \mu \nabla_{\perp}^2 B_z - \nu \nabla_{\perp}^4 B_z, \quad (6)$$

where now $\mathbf{v} = \mathbf{e}_z \times \nabla \phi + \mathbf{e}_z V_z$.

For all our calculations, the initial conditions are the same as those used by Ramos *et al.*¹¹ in their initial-value study of reconnection in VTF, except for a rotation of the fields by $\pi/4$ to align the generated current sheets with one of the coordinate directions: $\psi_0(x, y) = (B_{\infty}/2)(y^2 - x^2)$ and $\phi_0(x, y) = E_{\infty}/(4B_{\infty}) \ln[(y^2 + x^2) + \delta^2]/[(y^2 - x^2) + \delta^2]$, where δ is a regularizing parameter chosen to be larger than other relevant length scales. Note that since Ref. 11 uses an infinite spatial domain with different boundary conditions than employed here, a direct comparison of the results is not feasible. The (quasi) steady-state results are independent of the exact functional dependence of ϕ_0 and ψ_0 on δ , or on its exact value. In the HMHD model, we let $B_{z0}(x, y) = V_{z0}(x, y) = 0$. For computational reasons, the fields are written in the form $\psi(x, y, t) = \psi_0(x, y) + \tilde{\psi}(x, y, t)$, etc., with no assumptions on

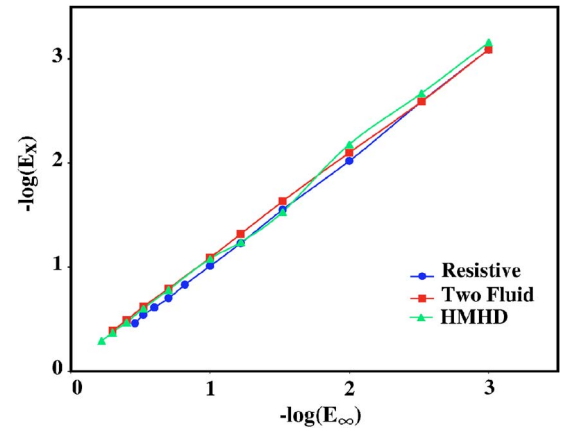


FIG. 2. (Color online) Reconnection rate as a function of the applied electric field. Purely resistive: $d_e = \rho_s = d_i = 0$ and $\eta = 10^{-3}$. Reduced two-fluid model: $d_e = 0.1$, $\rho_s = 0.2$, and $\eta = 10^{-3}$. Hall MHD model: $d_i = 0.2$ and $\eta = 10^{-3}$.

the magnitude of $\tilde{\psi}/\psi_0$. The boundary conditions for the time-dependent components are $\tilde{\phi} = \tilde{U} = \tilde{B}_z = 0$ and $\partial \tilde{\psi} / \partial n = \partial \tilde{F} / \partial n = \partial \tilde{J} / \partial n = \partial \tilde{V}_z / \partial n = 0$, where n represents the normal direction to the boundary. Note that for our purposes, the important difference between the two models above is that in the reduced two-fluid equations [Eqs. (1) and (2)], the small-scale dynamics is controlled by kinetic Alfvén waves, driven by the ρ_s term in Ohm's law, whereas in the HMHD model, this role is played by the whistler waves due to d_i terms.¹²

One of the main results of this work, the linear dependence of the reconnection rate on the external electric field E_{∞} , is shown in Fig. 2, where we plot the reconnection rate as a function of the applied electric field E_{∞} for $10^{-3} \leq E_{\infty} \leq 0.6$. (In dimensional units $E_{\infty}^{\text{dimen}} = v_A B_{\infty} E_{\infty}$.) The data were produced by incrementally increasing E_{∞} after a (quasi) steady state was reached at the previous value (an example is shown later in Fig. 4). The rate is measured by the electric field at the X point, calculated as $E_X \equiv -\partial \psi(x=0, y=0, t) / \partial t$. The plot shows the results from all three of the physics models mentioned above: the purely resistive case, the reduced two-fluid model, and the HMHD model. With some small variations, all three models exhibit the simple scaling law, $E_X \approx E_{\infty}$. This trivial point of course follows from the requirement for steady state in our two-dimensional geometry and constant electric field at the boundary. Thus, the (quasi) steady-state reconnection rate is determined by the external drive, regardless of the reconnection-layer physics.

This result precludes spurious scaling of E_X with other parameters in the system; within practical computational limits, it holds independently of the values chosen for various parameters such as d_e , d_i , ρ_s , and η . Thus, in *truly driven* reconnection, the only relevant parameter is the strength of the drive, and the dependence of E_X on any other variable seen in other contexts has to be attributed to an interaction of the reconnection region, as defined above in the introduction, with the region driving the reconnection, i.e., a lack of clear separation of the drive from the driven. Since this interaction is usually a complicated function of the geometry and details of the physics model, it is only natural that each model without this separation will lead to a different scaling of the re-

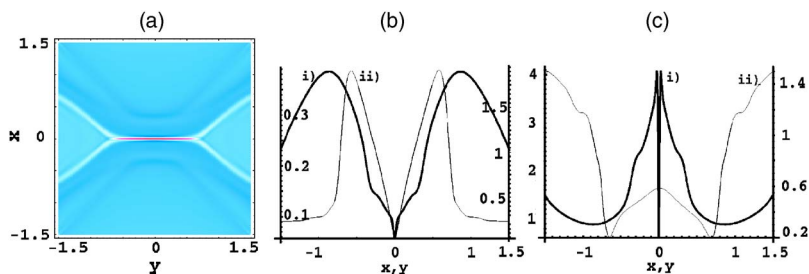


FIG. 3. (Color online) Global structure of the reconnection layer in the purely resistive case for $E_\infty=0.35$ and $\eta=10^{-3}$. (a) The current sheet. (b) Profiles of the inflow and outflow velocities. (i) Inflow, $|v(x, y=0)|$ (left vertical scale). (ii) Outflow, $|v(x=0, y)|$ (right vertical scale). (c) Profiles of the magnetic-field amplitude. (i) $|B(x, y=0)|$. (ii) $|B(x=0, y)|$.

connection rate with the applicable parameters. But clearly any such scaling law cannot be universal, and the only general statement that can be made in (quasi) steady-state driven reconnection is $E_X \simeq E_\infty$. Thus, the peak reconnection rate of $E \sim 0.24 B_0 v_A$ quoted by the GEM Challenge work¹³ for the Harris pinch problem and other similar claims^{14,15} have to be qualified by the specifics of the problem. In particular, although Ref. 15 also obtains rates independent of d_i , the asymptotic limit they observe has to be attributed to the absence of a separation of the drive and the reconnection dynamics in the sense outlined above.

Although all three physics models exhibit the simple scaling of the reconnection rate with the applied electric field, $E_X \simeq E_\infty$, details, in particular, those of the current sheets, differ markedly between the purely resistive model and the semicollisional/collisionless models. In the collisional case, where we used $\eta=10^{-3}$, $L=1.5$, and $B_\infty=1.5$, the well-known Sweet-Parker rate is $M_{SP}=(\eta/Lv_{A\infty})^{1/2}=2.1 \times 10^{-2}$. For $E_\infty < E_{SP} \equiv M_{SP}[v_{A\infty} B_\infty]=4.7 \times 10^{-2}$, reconnection proceeds without modifying the X -point geometry of the initial quadrupole field. For $E_\infty > E_{SP}$, however, the flux arrives at the layer faster than the rate of dissipation, and we enter the flux pileup regime,¹⁶ leading to an elongated current sheet, as extensively discussed by Biskamp.¹⁷ Figure 3(a) shows the highly extended structure of the current layer for $E_\infty=0.35$. The inflow velocity and field amplitude at the edge of the resistive layer are $v_{in} \simeq 0.1$ and $B_{in} \simeq 4$, as seen in panels (b) and (c) of Fig. 3. Unlike the usual Sweet-Parker model, these values are quite different from the asymptotic values at the boundary, $B_\infty=1.5$, and $u_\infty=E_\infty/B_\infty=0.23$. Note also that the outflow from the layer is nearly Alfvénic, with a peak velocity of $v_{max} \simeq 1.9$, which is approximately $2/3$ of the Alfvén speed at the edge of the layer. The electric field is uniform, $E_\infty=u_\infty B_\infty \simeq v_{in} B_{in} \simeq E_X$, and within the layer, it is balanced by the resistive term: $E_X \simeq \eta J_X$. The magnitude of the current and the geometry of the layer are quite different in this collisional model than those observed in the VTF experiment, which typically sees very little current.^{18,19}

Note that in a self-consistent (self-contained) problem, such as the evolution of the $m=1$ internal kink mode in tokamaks, the flux pileup observed here [Fig. 3(c)] would immediately reduce the potential energy available to the mode, i.e., slow down the drive, so that the nonlinear mode would evolve at the Sweet-Parker rate.²⁰

For $E_\infty \geq 0.35$, the extended current sheet eventually breaks up due to a tearing instability, which leads to a series of intermittent reconnection events.¹⁷ The reconnection rate in this regime becomes hard to quantify and is not examined further in this Letter. Note that this limit, $E_\infty=0.35$, is not universal but depends on various other parameters in the problem.

The observation $E_X \simeq E_\infty$ is easier to establish in the semicollisional/collisionless regimes using the reduced two-fluid or HMHD models, where the currents are mostly localized around the X point, and the numerical challenges associated with an extended current sheet do not arise. For the reduced two-fluid model, the geometry of the reconnection layer is shown in Fig. 4 for $E_\infty=0.4$. We note that, even with these strong drives ($M_\infty \equiv u_\infty/v_{A\infty}=0.4$), the layer essentially maintains the X -point geometry of the initial field. The outflow from the layer is through wide-open “nozzles” [Fig. 4(b), the red-colored regions], as first reported for a cylindrical $m=1$ mode in tokamaks using a similar physics model.²¹ We have been able to drive this system up to $E_\infty=0.5$ ($M_\infty=0.5$), beyond which poorly understood, large-amplitude oscillations in time corrupt the numerical results. A partial time history of the electric field at the X point, as it responds to incremental changes to the field at the boundary, is shown in Fig. 4(c).

The Hall MHD model calculations, despite the differences in physics governing the small-scale dynamics (whistlers here versus the kinetic Alfvén waves above), produce results similar to those obtained with the reduced two-fluid model. Figure 5 shows the global structure in the HMHD layer for $E_\infty=0.4$. The current layer is again localized around

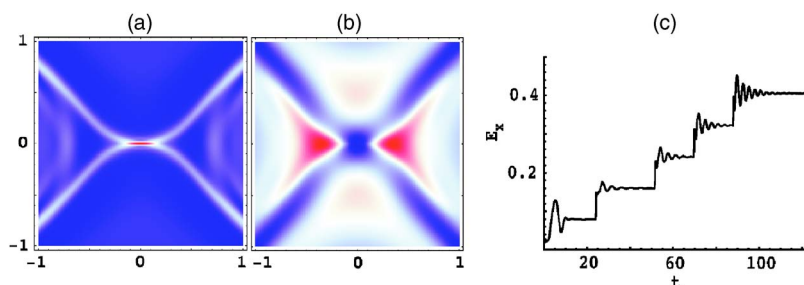


FIG. 4. (Color online) (a) The current sheet in the two-fluid model, for $E_\infty=0.40$, $d_e=0.1$, and $\rho_s=0.2$. (b) $v^2 = |\nabla\phi|^2$. (c) A partial time history of the electric field at the X point.

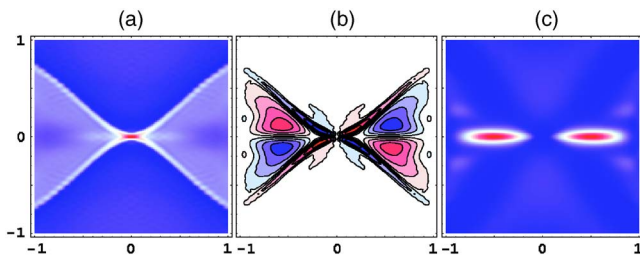


FIG. 5. (Color online) Global structure of layer in the Hall MHD model, for $E_\infty=0.40$ and $d_i=0.2$. (a) The current sheet. (b) Contours of B_z , the out-of-plane component of the field. (c) $v^2=|\nabla\phi|^2$.

the X point. The contours of the out-of-plane B_z field, due to whistlers and presumably responsible for maintaining the X -point structure of the layer,¹² are shown in Fig. 5(b). Interestingly, the outflow from the layer has the form of two well-collimated jets here [Fig. 5(c)], which differs from the flow in two-fluid model above [Fig. 4(b)], where it fans out following the contours of the opening separatrix. Note also that the two maxima in v^2 are located well outside the layer. This series of calculations was stopped at $E_\infty=M_\infty=0.6$ because of time constraints. We have not yet seen any physical or numerical limits on how hard this system can be driven.

As stated earlier, in the resistive calculations, the (quasi) steady-state current density in the layer is such that the electric field is balanced by the resistive term in Ohm's law: $E_X \approx \eta J_X$. For the reduced two-fluid and HMHD calculations, with similar spatial resolutions, the observed current-density amplitude is at least an order of magnitude lower and $E_X \gg \eta J_X$. (The resistivity for all three series of calculations was fixed at $\eta=10^{-3}$.) In the two-fluid model, the electron inertia terms lead to a well-known, cusp-like structure in J_z at the X point that cannot be fully resolved numerically—an effective dissipation level is set by numerics or the hyper-resistivity term. In the HMHD model, again there appear to be good physical reasons why the resistive term can never balance the electric field at the X point,²² and one has to invoke at least a fourth-order dissipation term (anomalous electron viscosity, or hyper-resistivity) to balance the reconnection field: $E_X \sim \nu \nabla_\perp^4 \psi$. Thus, the effective (or anomalous) resistivity at the X point is much higher than expected: $\eta_{\text{effect}} \equiv E_X/J_X \gg \eta$.

These observations in the collisionless regime are in qualitative agreement with the experimental results from VTF, where very little current (or equivalently, a very high anomalous resistivity) around the X point is seen.^{8,18,19} Invocation of a local anomalous electron viscosity to balance E_X in these fluid models is also consistent with the single-particle trapped-electron picture of Egedal;¹⁸ trapped-electron physics would manifest itself in a fluid model as anomalous viscosity entering through the off-diagonal terms of the pressure tensor. However, scaling of the layer width with the electron drift orbit size, as observed in Ref. 23, of

course cannot be reproduced in these fluid calculations. Similarly, η_{effect} , which determines the amount of current around the X point, is a strong function of the phenomenological constant ν (hyper-resistivity) in our model equations. A self-consistent determination of η_{effect} would require a kinetic treatment and is beyond the scope of this paper.

In summary, in 2D driven reconnection, when the drive is separated unambiguously from the reconnection region, the rate is determined by the boundary conditions, i.e., by the strength of the drive. The details of the physics model only determine the structure of the layer. With a collisional model, the current layer has the elongated “ Y -layer” configuration associated with slow reconnection, with the resistive term balancing the applied electric field. The collisionless models exhibit the “signature” configuration of fast reconnection, an “ X layer,” and the external field is balanced by the anomalous electron viscosity term in the generalized Ohm's law, leading to much lower current densities around the X point.

This work was supported by the U.S. DOE under Grant No. DE-FG03-96ER-54346. Computational resources were provided by the National Energy Research Scientific Computing Center, supported by the U.S. DOE under Contract No. DE-AC03-76SF00098.

¹D. Biskamp, *Magnetic Reconnection in Plasmas* (Cambridge University Press, Cambridge, 2000).

²E. Priest and T. Forbes, *Magnetic Reconnection, MHD Theory and Applications* (Cambridge University Press, Cambridge, 2000).

³D. Biskamp, E. Schwarz, and J. F. Drake, *Phys. Plasmas* **4**, 1002 (1997).

⁴A. Bhattacharjee, Z. W. Ma, and X. Wang, *Phys. Plasmas* **8**, 1829 (2001).

⁵P. A. Sweet, *Nuovo Cimento, Suppl.* **8**, 188 (1958).

⁶E. N. Parker, *J. Geophys. Res.* **62**, 509 (1957).

⁷H. E. Petschek, in *AAS/NASA Symposium on the Physics of Solar Flares*, ed. W. N. Hess (NASA, Washington, 1964), p. 425.

⁸J. Egedal, A. Fasoli, D. Tarkowski, and A. Scarabosio, *Phys. Plasmas* **8**, 1935 (2001).

⁹T. J. Schep, F. Pegoraro, and B. N. Kuvshinov, *Phys. Plasmas* **1**, 2843 (1994).

¹⁰R. Fitzpatrick, *Phys. Plasmas* **11**, 937 (2004).

¹¹J. J. Ramos, F. Porcelli, and R. Verástegui, *Phys. Rev. Lett.* **89**, 055002 (2002).

¹²B. N. Rogers, R. E. Denton, J. F. Drake, and M. A. Shay, *Phys. Rev. Lett.* **87**, 195004 (2001).

¹³J. Birn, J. F. Drake, M. A. Shay, B. N. Rogers, R. E. Denton, M. Hesse, M. Kuznetsova, Z. W. Ma, A. Bhattacharjee, A. Otto *et al.*, *J. Geophys. Res.* **106**, 3715 (2001).

¹⁴D. Biskamp, E. Schwartz, and J. F. Drake, *Phys. Rev. Lett.* **75**, 3850 (1995).

¹⁵M. A. Shay, J. F. Drake, M. Swisdak, and B. N. Rogers, *Phys. Plasmas* **11**, 2199 (2004).

¹⁶E. R. Priest, *Rep. Prog. Phys.* **48**, 955 (1985).

¹⁷D. Biskamp, *Phys. Fluids* **29**, 1520 (1986).

¹⁸J. Egedal, *Phys. Plasmas* **9**, 1095 (2002).

¹⁹J. Egedal, W. Fox, and M. Porkolab, *Phys. Plasmas* **11**, 2844 (2004).

²⁰A. Y. Aydemir, J. C. Wiley, and D. W. Ross, *Phys. Fluids B* **1**, 774 (1989).

²¹A. Y. Aydemir, *Phys. Fluids B* **4**, 3469 (1992).

²²M. A. Shay, J. F. Drake, B. N. Rogers, and R. E. Denton, *J. Geophys. Res.* **106**, 3759 (2001).

²³J. Egedal, A. Fasoli, and J. Nazemi, *Phys. Rev. Lett.* **90**, 135003 (2003).